Modeling of acoustical porous materials under flow

F. Chevillotte[1], M. Martinez[1], F.-X. Bécot[1], L. Jaouen[1]

1: Matelys – Research Lab., 7 rue des Maraîchers, Bât. B, 69120 Vaulx-en-Velin, France

Abstract: Acoustical porous materials are commonly used to reduce the noise in the presence of flow. In such applications, it is essential to control how these materials may alter the flow and may re-generate noise.

The purpose of this work is to show different ways to take into account the porous materials in Computational Fluid Dynamics (CFD) simulations and how CFD simulations can help to characterize the behavior of porous media under flow.

This paper focuses on the use and the coupling between porous media and Lattice Boltzmann Method (LBM).

Keywords: Porous media, flow, LBM

1. Introduction

Porous media are used in CFD simulations to calculate the drag coefficient (e.g. heat exchanger) and the acoustical energy dissipation (liners, mufflers ...)

Usually, the use of the airflow resistance is sufficient to model the viscous force induced by the porous medium for aerodynamic purposes whereas the modeling of the acoustical energy dissipation requires more parameters. Robust porous models are proposed in the literature but they are generally defined in the frequency domain while the CFD methods are solved in the time domain.

First, the CFD method is presented. Then, the modeling principles of the dissipation of acoustic energy in porous media without flow are recalled. The consequences in the presence of flow are then presented and discussed.

This work, for which the LBM is used for CFD simulations, consists in three axes:

(i) Predicting the macro-properties of a porous material under the flow from the description of its micro-structure (see Figure 1),

(ii) Modeling of porous media using the surface impedance (see Figure 2: bottom),

(iii) Modeling of porous media using a bulk representation (see Figure 2: top).

Finally, advantages and drawbacks of the presented methods will be discussed.

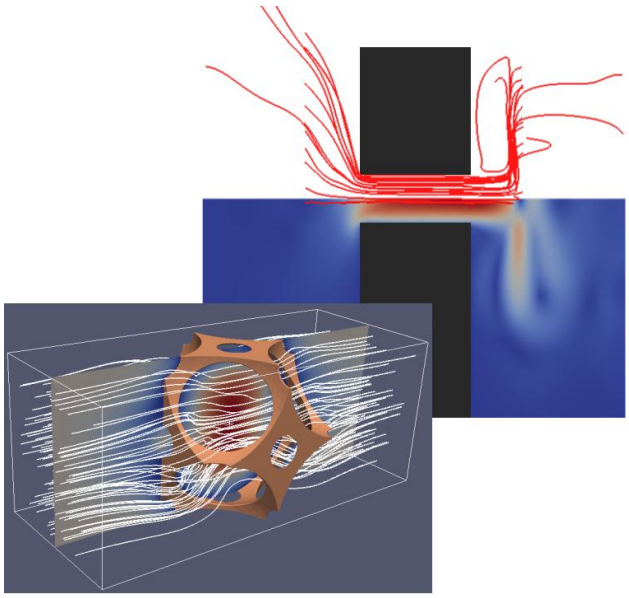

Figure 1: Typical flow profile at the microscopic scale within a porous media.

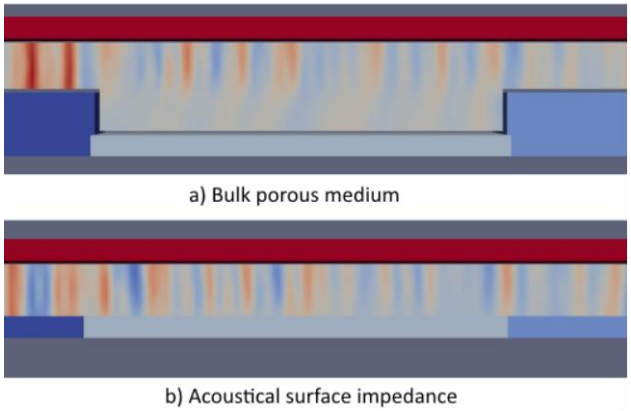

Figure 2: Density field of a tunnel with a liner modeled as (a) a bulk porous medium and (b) an acoustical surface impedance.

2. Description of the CFD method

The Lattice Boltzmann solver named “LaBS" [1] has been used for all simulation results shown throughout this paper. This brand new code has been developed within a consortium of industrial companies (Renault, Airbus, CS), academic laboratories (UPMC, ENS Lyon) and strong partnerships with other entities (Onera, Alstom, Paris Sud University, Gantha, Matelys) from 2010 to 2014.

LaBS is built upon the classical Lattice-Boltzmann principles [2] and uses a D3Q19 lattice, with a two-relaxation-time collision model for a better robustness / accuracy tradeoff [3].

Turbulence is handled according to LES approach [4], either with high order explicit filtering (Approximate Deconvolution Model [5]) or with a dedicated subgrid scale model (Shear Improved Smagorinsky Model [6]).

Near-wall-turbulence is modelled using wall laws accounting for adverse pressure gradient effects [7] and curvature effects.

Special care has been paid on two numerical ingredients crucial for aeroacoustic applications:

- The dissipation and dispersion [8] are kept as low as possible to enable proper generation & propagation of acoustic waves.
- The computational domain boundary conditions use absorbing layers [9, 10] to avoid spurious acoustic waves reflections.

More details about the LaBS solver as well as elementary validation cases can be found in a recent publication [11].

3. Modeling of acoustical porous media without flow

Considering long wavelength compared to the characteristic size of the pores, the acoustic propagation and the dissipation through a rigid porous media may be represented macroscopically by an equivalent fluid.

Using semi-phenomelogical models, the visco-thermal dissipation of acoustical energy through porous media is taken into account from two complex frequency-dependent functions (the dynamic density $\tilde{\rho}_{eq}(\omega)$ and the dynamic bulk modulus $\tilde{K}_{eq}(\omega)$, which are analytically derived from macroscopic parameters.

The most popular semi-phenomenological models are the Johnson-Champoux-Allard (JCA) and the Johnson-Champoux-Allard-Lafarge (JCAL) models. Johnson *et al.* [12] derived the visco-inertial effects from macroscopic parameters. Similarly, Champoux and Allard [13] derived the thermal effects. Lafarge *et al.* [14] improved the thermal response. A synthesis of JCA and JCAL models can be found in [15].

The usual macroscopic parameters are:

- ϕ the open porosity,
- σ the static airflow resistivity,
- Λ the viscous characteristic length,
- Λ' the thermal characteristic length,
- α_∞ the high frequency limit of tortuosity,
- k_0' the static thermal permeability.

The characteristic impedance $\tilde{Z}_c(\omega)$ and wavenumber $\tilde{k}_c(\omega)$ are obtained from the dynamic density and the dynamic bulk modulus.

The acoustical surface impedance (time convention $+j\omega t$) of a porous media of thickness t backed by a hard wall is written:

$$\tilde{Z}_s(\omega) = -j\tilde{Z}_c \tan^{-1}(\tilde{k}_c t) \quad [1]$$

and the sound absorption coefficient α is:

$$\alpha(\omega) = 1 - \left|\frac{\tilde{Z}_s - Z_0}{\tilde{Z}_s + Z_0}\right|^2 \quad [2]$$

with Z_0 the impedance of air.

4. Modeling of porous media under flow

4.1 Non-linear regime behavior

Basically, the porous media are taken into account in Navier-Stokes equation as a body force $\vec{f}$:

$$\frac{\partial \vec{u}}{\partial t} + \vec{u} \cdot \nabla\vec{u} = -\frac{1}{\rho}\nabla \mathrm{p} + \upsilon\nabla^2\vec{u} + \vec{f} \quad [3]$$

where $\vec{f}$ is proportionnal to the velocity $\vec{u}$ and the airflow resistivity σ

$$\vec{f} = -r\vec{u} = -\frac{\sigma}{\rho}\vec{u} \quad [4]$$

The airflow resistivity σ is an intrinsic parameter of the porous media and r, which is the airflow resistivity normalized by the density, is commonly used as input parameter in CFD computations.

Many porous materials delaminate when subjected to a flow. When dealing with a flow, the most used porous materials are perforated plates coupled to cavity or honeycombs. These materials are known to have a non-linear behavior which is taken into account by the total normalized airflow resistivity r_t:

$$r_t = r_0 + r_i|\vec{u}| \quad [5]$$

Melling [16] has studied this non-linear effect for perforated plates submitted to a high sound pressure level and has shown that the airflow resistance may be written as:

$$R_t = R_{lin}(L_p) + \frac{c_0}{2}\frac{8}{3\pi}\frac{1}{C_d^2}\frac{1-\phi^2}{\phi^2}U \quad [6]$$

The airflow resistance R_t is the product of the airflow resistivity σ by the thickness L_p. In the previous formula, the total resistance is the sum of a linear term R_{lin} and a non-linear term. The non-linear term is proportional to the upstream velocity level U and depends on the open porosity ϕ and a discharge

coefficient C_d. This latter coefficient is usually obtained from experiments.

4.2 Predicting the macro-properties of a porous media under flow from the description of the microstructure

In this section, the ability to evaluate the linear and non-linear terms of Eq. [5] from the microstructure is investigated. Figure 3 shows the flow distortion around a perforation for three velocity levels and the airflow resistivity is plotted as a function of the upstream velocity in Figure 4. The perforated plate has a thickness L_p of 2 mm, a hole diameter d of 1 mm and a perforation rate ϕ of 0.008.

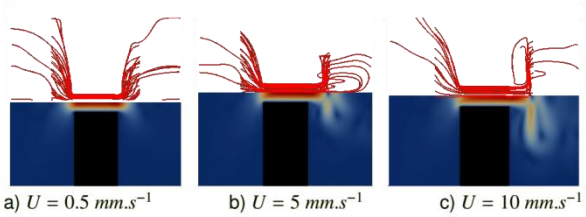

Figure 3: Flow distorsion around a perforation for three velocity levels ($d = 1$ mm, $L_p = 2$ mm, $\phi = 0.008$).

It can be seen that the dowstream flow distorsion strongly increases with the velocity level. The quasi-static airflow resistivity can be measured according to the standard ISO 9053 [17] which recommends a velocity level of 0.5 mm/s.

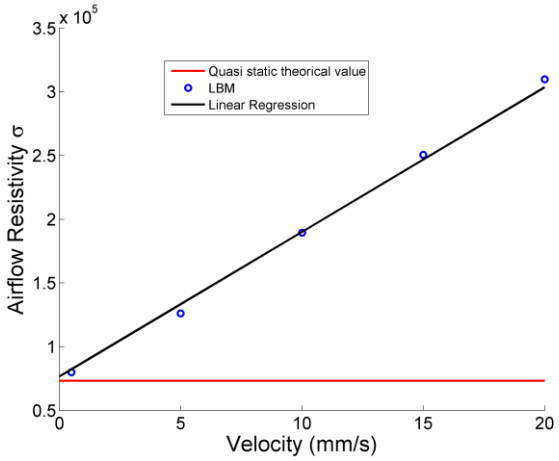

Figure 4: Airflow resistivity as a function of the upstream velocity.

The linear regression enables to determine the quasi-static limit of the airflow resistivity. This regression method may also be used experimentally if the device does not allow performing the measurement at 0.5 mm/s.

The dissipation phenomena involved around a perforation can be separated as inner viscous effects in the perforation and additional viscous effects upstream and downstream the perforation as depicted in Figure 5. Note that additional viscous effects also appear in the linear regime (at low Reynolds) and are taken into account as a length correction.

The total resistance is thus the sum of the resistance due to inner viscous effects R_p and the additional viscous effects R_r:

$$R_t(\phi, L_p, U, d) = R_p(\phi, L_p, U, d) + R_r(\phi, U) \quad [7]$$

The resistance R_p induced by the inner effect depends on the velocity in the hole U/ϕ, the diameter of the hole d and is proportional to the thickness of the perforation L_p. Eq. 7 can be expressed as a function of the airflow resistivity due to the inner viscous effects σ_p:

$$R_t(\phi, L_p, U, d) = \sigma_p(\phi, U, d)L_p + R_r(\phi, U) \quad [8]$$

The additional resistance R_r mainly depends on the velocity in the hole U/ϕ and the distance between holes which is included in the perforation rate ϕ.

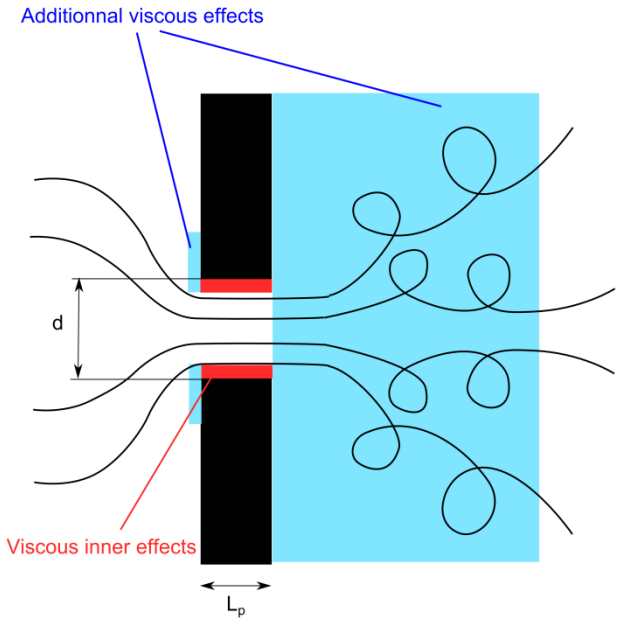

Figure 5: Scheme of the flow distorsion and viscous phenomena around a perforation.

Both the inner and the additional viscous effects may have a non-linear behavior. The total resistance can potentially depend on four terms:

$$R_t = (\sigma_{p0} + \sigma_{pi}|U|)L_p, + R_{r0} + R_{ri}|U| \quad [9]$$

A parametric study has been carried out in order to determine these latter coefficients. The perforation thickness varied in the range [0.5 - 5 mm], the perforation diameter in the range [0.5 - 4 mm] and the perforation rate in the range [0.0314 - 0.503].

The total resistance is plotted as a function of the thickness of the perforation in Figure 6 for four upstream velocity levels (0.5, 20, 30 and 50 mm/s) and behaves as affine function.

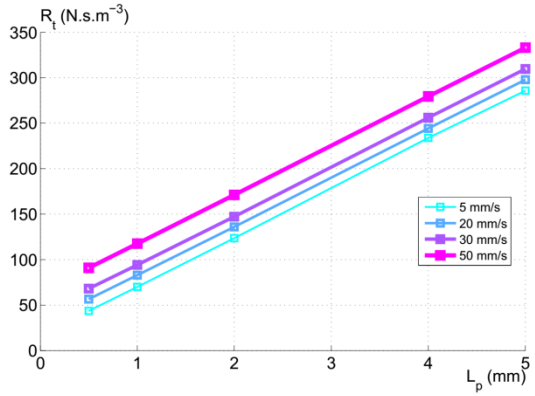

Figure 6: Total airflow resistance as a function of the thickness of the perforation for four upstream velocity levels.

The ordinates correspond to the added resistance R_r and the slopes are the airflow resistivity due to inner effects σ_p. These two quantities are presented in Figure 7 and 8.

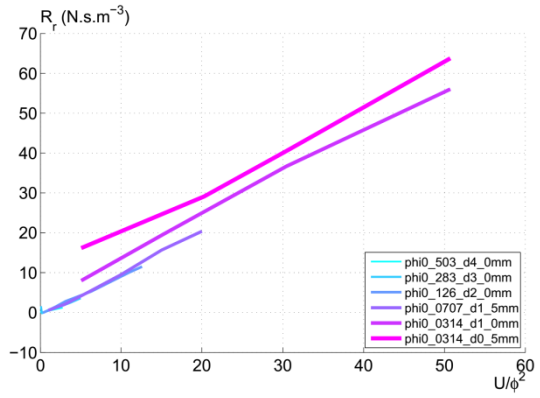

Figure 7: Added resistance as a function of U/ϕ^2.

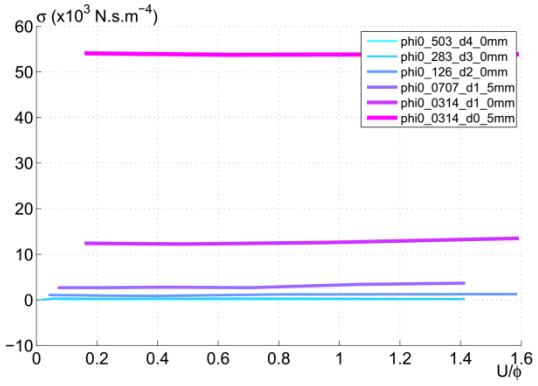

Figure 8: Airflow resistivity as a function of the velocity in the hole U/ϕ.

These results show that the inner viscous effects do not have a non-linear behavior for this range of upstream velocity. The non-linear behavior strongly depends on the downstream flow distorsion and seems to be proportionnal to the ratio U/ϕ^2.

Finally, these results confirm the equation [6] proposed by Melling and this numerical methodology can be used in order to determine the discharge coefficient C_d.

4.3 Modeling of porous media using surface impedance

At the scale of a full system (automotive, aircraft ...), it is not reasonable to mesh the entire microstructure of the porous media. The simplest method is to use acoustical surface impedance. This method allows taking into account locally reacting material (e.g. perforated plates combined with honeycomb) but does not considered the flow through the porous medium.

Two difficulties must be circumvented in the implementation of such a method:

- The surface impedance must be expressed in the time domain whereas the most advanced impedance models are expressed in the frequency domain.
- The classical CFD boundary conditions impose the velocity or the density whereas the impedance boundary condition imposes the ratio between density and velocity.

The time-domain surface impedance model proposed by Özyörük *et al.* and is used [18].

This impedance model can be expressed in the frequency domain as an assembly of low-pass, pass-band and high-pass filters and requires 7 coefficients z_i:

$$\frac{Z(\omega)}{\rho_0 c_0} = z_1 + \frac{z_2 - z_1}{1 + i\omega z_3} + \frac{i\omega z_4}{(1 - \omega^2/z_6) + i\omega z_5} + i\omega z_7 \quad [10]$$

The corresponding impedance model in the z-domain writes:

$$Z(z) = \frac{\sum_{l=0}^{4} a_l z^{-l}}{-\sum_{k=0}^{3} b_k z^{-k}} \quad [11]$$

The coefficients a_i and b_i are identified from the z_i coefficients and the time step dt.

The impedance condition can be written at time *i+1*:

$$a_0 v^{i+1} - c_0^2 \rho^{i+1} = c_0^2 \sum_{k=0}^{3} (b_k - b_{k+1})(\rho^{i-k} - \rho_0) + \sum_{l=0}^{4} (a_l - a_{l+1}) v^{i-l} - c_{0\rho_0}^2 \quad [12]$$

with v the normal velocity relative to the mean flow, ρ_0 the density of air and c_0 the speed of sound. This model requires storing the five last time steps and an estimation of the mean flow [10].

A surface impedance model has been implemented in the Lattice Boltzmann method as previously carried out by Toutant and Sagaut [19] or Sun *et al.* [20].

4.4 Modeling of porous media using a bulk representation

The complete modeling of a porous media for aerodynamical and acoustical purposes requires a bulk modeling where the material would be seen as an equivalent fluid (as for rigid porous media without flow).

It can be shown that the equivalent fluid model of the usual porous model, which only takes into account the airflow resistivity, may be expressed as:

$$\tilde{\rho}_{eq}(\omega) = \rho_0 \left(1 + \frac{\sigma}{i\omega\rho_0}\right) \quad [13]$$

$$\tilde{K}_{eq}(\omega) = \gamma P_0 \quad [14]$$

This simple model does not allow representing the frequency behavior of conventional acoustical porous media. The bulk representation should at least take into account the open porosity ϕ and the tortuosity α_∞. The corresponding 3-parameter equivalent fluid model becomes:

$$\tilde{\rho}_{eq}(\omega) = \frac{\rho_0 \alpha_\infty}{\phi}\left(1 + \frac{\sigma\phi}{i\omega\rho_0\alpha_\infty}\right) \quad [15]$$

$$\tilde{K}_{eq}(\omega) = \frac{\gamma P_0}{\phi} \quad [16]$$

This requires replacing the density of air ρ_0 by $\rho_0\alpha_\infty/\phi$ in the volume. The continuity of the velocity is easily ensured but a special treatment must be applied at the interface (Figure 9) between the air and the porous medium to ensure the continuity of the normal stress as carried out by Bai *et al*. [21] in a Lattice Boltzmann framework.

$$u_{fluid} = u_{porous} \quad [17]$$

$$v \left.\frac{\partial u_n}{\partial n}\right|_{fluid} = \frac{v}{\phi} \left.\frac{\partial u_n}{\partial n}\right|_{porous} \quad [18]$$

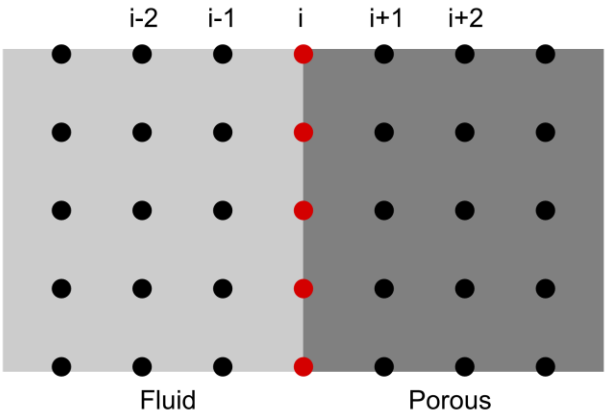

Figure 9: Interface between flluid (air) and porous medium in lattice Boltzmann scheme.

5. Results

5.1 Effect of the pressure level on the sound absorption coefficient

The perforated plate backed by a cavity can show a non-linear behavior when submitted to a high--sound pressure level under normal incidence. The mean upstream velocity can be estimated for each sound pressure level and the airflow resistance of the plate is adjusted thanks to Eq. 6 and the discharge coefficient obtained using the methodology proposed in section 4.2.

The sound absorption coefficient of a 1 mm-thick plate with a perforation diameter of 1 mm, a perforation rate of 0.0314 and backed by a 20 mm-thick air cavity is plotted in Figure 10 for sound pressure levels in the range [100 - 150 dB].

The non-linear regime appears around 120 dB for this configuration.

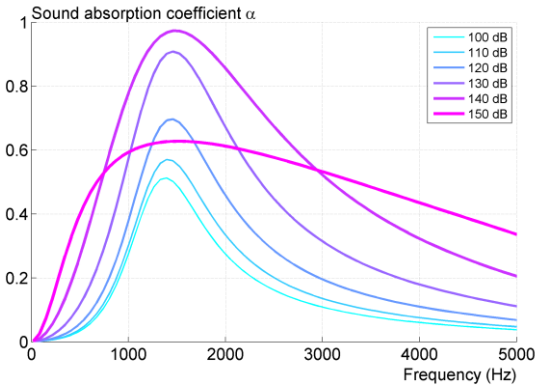

Figure 10: Sound absorption coefficient of a perforated plate backed by an air cavity at different sound pressure levels

5.2 Liner configuration

The bulk porous medium and the surface impedance models are now compared using a liner configuration. This latter configuration is a straight duct with a length of 4 m and a height of 50 mm. The porous liner has a length of 38 cm and a thickness of 40 mm. A white noise is imposed at the inlet, (eventually in addition to a mean flow) and a non-reflective boundary condition is set at the outlet.

The density fluctuations $\rho - \rho_0$ and the normal velocity are shown in Figure 11 and 12 using the bulk porous medium model and the corresponding surface impedance for 0 and 85 degree incidence.

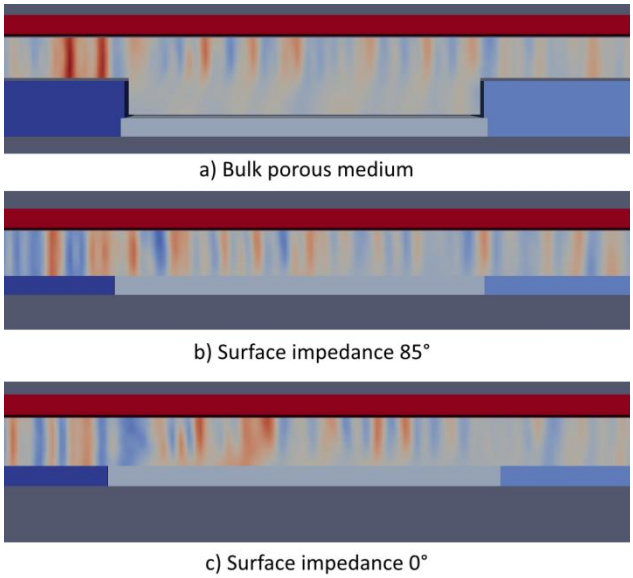

Figure 11: Density fluctuations $\rho - \rho_0$ for the liner configuration with a) bulk porous medium, b) normal-incidence acoustical surface impedance and c) 85-degree incidence acoustical surface impedance (without mean flow).

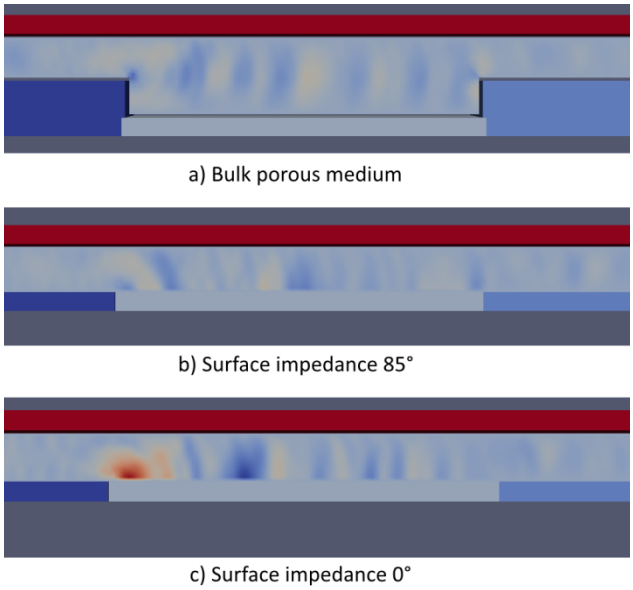

Figure 12: Normal velocity for the liner configuration with a) bulk porous medium, b) normal-incidence acoustical surface impedance and c) 85-degree incidence acoustical surface impedance (without mean flow).

The Figures 11 and 12 show that the normal incidence (0°) acoustical surface impedance model is far from the bulk porous medium model whereas the 85-degree-incidence surface impedance tends to the same behavior.

This result can also be observed in terms of insertion loss in Figure 13. The impedance models give similar results with or without the mean flow. Which means the impedance model is well applied on the fluctuating fields (density and velocity). As expected, the interaction between the flow and the porous medium modifies the acoustical behavior.

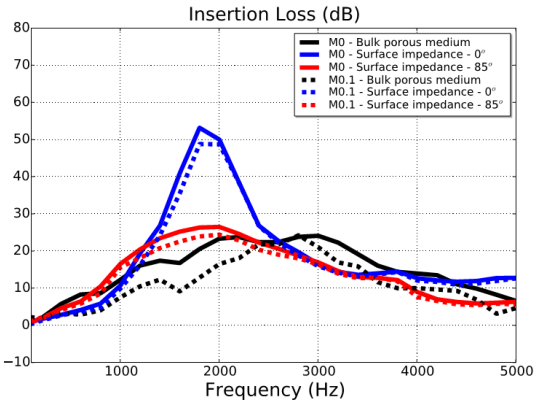

Figure 13: Insertion loss (dB) velocity for the liner configuration with a) bulk porous medium, b) normal-incidence acoustical surface impedance and c) 85-degree incidence acoustical surface impedance (with and without mean flow).

6. Conclusion

This work presented three methods to take into account the porous media in Lattice Boltzmann method. Of course, each method has advantages and drawbacks.

The modeling at the scale of the microstructure allows determining the representative macroscopic parameters and particularly the airflow resistance. The discharge coefficient, usually obtained experimentally, can thus be numerically estimated. This microscopic modeling is too much time and memory consuming when dealing with a full system such an automotive or an aircraft.

The acoustical impedance modeling enables to consider complex locally reacting behavior without meshing the porous media. The surface impedance model suggested by Özyörük seems robust enough if the frequency fit is carefully achieved in order to ensure the causality of the filter.

Finally, the more accurate modeling is the 3-parameter bulk representation which allows taking into account both the acoustical behavior of conventional porous media and the flow passing through. Future works will focus on the improvement of this bulk modeling in terms of precision and robustness.

7. Acknowledgement

The present work has been supported by French funded projects LABS & CLIMB in the framework of the "Programme d'Investissement d'Avenir: Calcul Intensif et Simulation Numrique".

7. References

[1] "Lattice-Boltzmann Solver LaBS," http://www.labs-project.org, 2014

[2] Chen, S. and Doolen, G., "Lattice Boltzmann Method for fluid flows," Ann. Rev. Fluid Mech. , Vol. 30, 1998, pp. 329-364.

[3] Ricot, D., Foquet, E., Touil, H., Lévêque, E., Machrouki, H., Chevillotte, F., and Meldi, M., "Aeroacoustic computations with new CFD solver based on Lattice Boltzmann Method," Automotive and railway Comfort , Le Mans, France, 2012.

[4] Sagaut, P., *Large Eddy Simulation for incompressible*
ows, Scientific computation series, Springer-Verlag, 2000.

[5] Malaspinas, O. and Sagaut, P., "Advanced large-eddy simulation for lattice Boltzmann methods: The approximate

deconvolution model," Phys. Fluids , Vol. 23 - 105103, 2011.

[6] Lévêque, E., Toschi, F., Shao, L., and Bertoglio, J.-P., "Shear-improved Smagorinsky model for large-eddy simulation of wall-bounded turbulent flows," J. Fluid Mech., Vol. 570, 2007, pp. 491-502.

[7] Afzal, N., "Wake layer in a turbulent boundary layer with pressure gradient- A new approach," IUTAM Symposium on Asymptotic Methods for Turbulent Shear Flows at High Reynolds Numbers, Bochum, Germany, 1996, pp. 95-118.

[8] Ricot, D., Marié, S., Sagaut, P., and Bailly, C., "Lattice Boltzmann method with selective viscosity filter," J. Comput. Phys. , Vol. 228, 2009, pp. 4478-4490.

[9] Xu, H. and Sagaut, P., "Analysis of the absorbing layers for the weakly-compressible lattice Boltzmann methods," J. Comput. Phys. , Vol. 245, 2012, pp. 14-42.

[10] Chevillotte, F., Ricot, D., "Development and evaluation of non-reflective boundary conditions for lattice Boltzmann method", 22nd AIAA/CEAS Aeroacoustics Conference, AIAA 2016-2915.

[11] Touil, H., Ricot, D., and Lévêque, E., "Direct and large-eddy simulation of turbulent flows on composite multi-resolution grids by the lattice Boltzmann method," J. Comput. Phys. , 2014, pp. 220-233.

[12] Johnson D.L., Koplik J., and Dashen R., "Theory of dynamic permeability and tortuosity in fluid-saturated porous media", J. Fluid Mech., 379-402 (1987).

[13] Champoux Y. and Allard J.F., "Dynamic tortuosity and bulk modulus in air-saturated porous media", J. Appl. Phys. 70, 1975-1979 (1991).

[14] Lafarge D., Lemarinier P., Allard J.F., and Tarnow V., "Dynamic compressibility of air in porous structures at audible frequencies", J. Acoust. Soc. Am. 102, 1995-2006 (1997).

[15] Allard J.F., Atalla N., Propagation of sound in porous media. Modeling sound absorbing materials,(Wiley, Chichester, UK, 2009),2nd Ed., Chap 5., 358 pages.

[16] Melling, T.H., "The acoustic impedance of perforates at medium and high sound levels," J. Sound. Vib., Vol. 29(1), 1973, pp. 1-65.

[17] ISO 9053, Acoustics - Materials for acoustical application - Determination of airflow resistance, 1991

[18] Özyörük, Y., Long, L. N., and Jones, M., "Time-domain numerical simulation of a flow impedance tube," J. Comput. Phys., Vol. 146, 1998, pp. 29-57.

[19] Toutant, A. and Sagaut, P., "Lattice Boltzmann simulation of impedance tube flows," Computers & Fluids, Vol. 38, 2009, pp. 458-465.

[20] Sun, C., Pérot, F., Zhang, R., Freed, D., and Chen, H., "Impedance Boundary Condition for Lattice Boltzmann Model," Commun. Comput. Phys., Vol. 13, No. 3, 2013, pp. 757-768.

[21] Bai H., Yu P., Winoto S.H. and Low H.T., "Lattice Boltzmann method for flows in porous and homogeneous fluid domains coupled at the interface by stress jump," Int. J. Numer. Meth. Fluids 2009.

8. Glossary

CFD: Computational Fluid Dynamics

LBM: Lattice Boltzmann Method